



DESIGN AND IMPLEMENTATION OF A LOW COST, HIGH PERFORMANCE IONIZING RADIATION SOURCE DETECTION AND SOURCE DIRECTION FINDING SYSTEM

Burak ÇUHADAROĞLU¹ and Hakkı Gökhan İLK¹

¹Department of Electrical and Electronics Engineering, Ankara University, Ankara, TURKEY

ABSTRACT. This study shows the design, implementation, and test results of a low-cost portable radiation-detector system relies on a directionally designed multi detector probe that works in Geiger-Müller counting mode with a single chip solution. The proposed system can perform the functions of detecting the ionizing radiation source, counting gamma and showing the direction and angle of the gamma source relative to the position of the device. The radiation direction finding (RDF) system consists of a radiation probe and electronic sections that are mounted in a metal box. The probe has a cast housing made of lead material and it has 8 directional slots for placing the optically isolated PIN diode arrays where each array consists of 4 parallelly connected BPW 34 PIN model diode. The lead housing also blocks incident rays from unintended directions and provides a directional sensing for PIN diodes. The metal box contains 8 low noise amplifiers and pulse shaping detector boards that are assigned to each channel of PIN diode arrays, a signal inverter board, a step-up high voltage board, a 12 V battery and a parallel processing FPGA board with an embedded VHDL software that can process all 8 channels simultaneously and execute the direction estimation algorithm. The system also has an adjustable detector bias voltage and the applied voltage can be displayed on a seven-segment display located in front of the unit so that different models of PIN diodes can be used and tested with different bias voltage levels. It also has a HMI touch screen unit and user interface for displaying the Cpm or Cps values of each channel; a 360-degree scale showing the direction of the source with its pointer and an indicator showing the direction of the source numerically in degrees. The system works as a gamma detector and the source direction can also be detected within $\pm 45^\circ$ interval. The success of system within this interval is 99.22%. The detector was tested with low to high energy gamma sources (^{241}Am , 9.761 μCi , 59.54 keV, ^{137}Cs 661, 3.7 MBq, keV and ^{60}Co , μCi , 1173 and 1332 keV) and showed good sensitivity performance level in gamma ray detection. The major

Keywords. Radiation direction detection, gamma detection, nuclear electronics, embedded systems, detector design, nuclear detector

 burakcuhadaroglu@gmail.com-Corresponding author; ilk@ankara.edu.tr
 0000-0002-1067-0716; 0000-0003-4365-8286

outcome of this study and the major contribution of this work to the literature is therefore is the design and production details of a hand-held detector and source direction locator prototype; which is a light, portable and compact system.

1. INTRODUCTION

Gamma radiation sources are widely used in metal-encapsulated forms for medical, industrial and research purposes and they are subject to government regulatory control for public health and security. Spent and orphan sources may be harmful to unaware people; should be immediately detected and held by the trained and equipped search teams that will provide source safe until collection and off-site transport. Moreover, other gamma ray sources that are stolen, lost, abandoned, misplaced, unknown owner sources and illegally transferred or stored, and sources intentionally obtained by terrorists also cause safety risk. For safety reasons scrap metal recycling, custom offices, border controls or Nuclear Agencies use gamma detectors for searching lost isotopes, radioactive materials or radioactive contaminations and detecting the gamma ray leakage in nuclear facilities. Remote sensing of nuclear accidents and gamma rays' arrival angle estimation is an important parameter in these radiation monitoring and detection applications. A standard radiation source searching project requires to know dose and time duration that the person will be exposed to gamma ray and a team equipped with shielded clothes and detectors and active personal dosimetry. Existing systems provide energy and pattern change in indicated values. The surveyors should detect the position of the gamma source by personal skills and estimation and this increases the exposure time and dose to be received [1]. Compton cameras, which are mostly employed in the astrophysics area, count-based systems, collimators, and coded aperture systems are the three broad categories for gamma source direction determination. Two-dimensional semiconductor Germanium Strip Detectors (GSD) are used in high energy astrophysics fields by measuring energy and position of interactions and having better energy resolution and imaging than typical germanium detectors [2]. The spatial resolution in a device with 1 cm thickness is almost 200 μ m and limited by strip pitch of the device and the lateral dispersion of the charge cloud after an interaction [3]. Imaging gamma-ray detectors with double-sided germanium detector sensitive polarimeters use the Compton scattering cross-angular section's dependency on polarized gamma rays and the distribution of scatter orientations within the detector and optimized Compton polarimeters give more sensitive results [4]. In addition to GSD, thick microstrip 3D multilayer detectors having the advantage of lower doppler broadening by its low Z and capable of observing three Compton scatter technique are used in high resolution position sensitive detectors with low power ASICs capable of handling large number of channels connected to the arrays of microstrip detectors were developed in Naval Research Laboratory

(NRL) [5]. The advanced gamma-ray tracking-based Compton cameras have superior sensitivity in imaging gamma-ray sources than collimator-based systems and also increase the sensitivity for finding gamma-ray sources mainly in complex radiation fields, over the other non-imaging type detectors [6]. Based on the high purity germanium (HPGe) systems, the Advanced GAMMA Tracking Array (AGATA) was developed in Europe with the participation of more than 10 countries [7] and also in the USA, the Gamma Ray Energy Tracking Array (GRETA) was developed [8]. The HPGe detectors that are 100-200 highly segmented were placed in the system with a 4π geometry. By using the measured information and energy from the interaction points the paths are reconstructed by using developed reconstruction and backscattering algorithms [9]. Another suggested system is wind rose type gamma detector having dozens of scintillators and a position sensitive photo multiplier tube (PSPMTs) that could identify only lateral directions and a detector with two NaI (TI) scintillators with a triangle shape lead shield with the disadvantage of identifying the most significant incident angle was suggested. Various types of detectors' designs including a design similar to our device design, a spherical designed honeycomb-type detector system consisting of many scintillator pieces, a PSPMT and light guides was suggested for this purpose [10]. A system with a lead shield having special shape, a NaI (TI) scintillator with 3" x 3" dimensions and software was developed tested by rotating the shield 90° for 10-20 minutes and taking four measurements of energy spectra for one local position [11]. The Soft Gamma-ray Detector (SGD) is a Compton telescope developed in NeXT (Japanese future high energy astrophysics mission) that consist of a hybrid silicon and CdTe having a narrow field of view (FOV). This detector has background rejection gamma ray polarization measurement and high angular resolution capabilities by using Compton kinematics [12]. A designed gamma-ray detector for direction-finding purpose with three pieces of NaI (TI) and CsI (TI) scintillators and three photomultipliers; which was placed in a cylindrical housing with 120° could measure gamma ray energy and count. The incident angle was calculated by counting weight-based algorithm [13]. A similar system with the same structure having NaI (TI) scintillator system was also designed and gamma sources within 60-1250 KeV energy were measured the algorithms based on the weight of each detector counts to the total counts with $\pm 3^\circ$ angles. The resolution was less with respect to the previous design [14]. An approach by using two measurements with segmented gamma scanner (SGS) in opposing directions were evaluated and recommended for use by waste disposal regulators for the assay of radioactive waste drums primarily composed of organic materials [15]. Another gamma vector camera (GVC) that also can measure the direction of the neutron sources by using double neutron scattering and calculating the statistical mean of the incidence direction of the scattered neutron was developed with the help of DARPA by using polystyrene fibers and observed

by CCD (charge coupled device) cameras and additional image intensifiers. The system was tested by GEANT4 simulations [16]. Another system having three NaI detector placed in a housing connected to photomultiplier tubes, ADC blocks measuring the pulse heights of each detector a low power single CMOS chip that calculates the angle of incidence by using the proposed algorithm within 5° [17]. Another three-dimensional position-sensitive semiconductor detector was developed using the generalized likelihood ratio test (GLRT). Using the combined energy and direction information from these detectors, the source-intensity test (SIT) is used to automate the detection and identification of point sources of radiation in the diffused background. SIT outperformed commercial software Genie 2000 (Canberra) [18]. A system was suggested with the three-perpendicular quadratic NaI scintillator array placed perpendicular to each other for determining the incidence angle of cosmic rays and simulations in GEANT performed small variations [19]. A circular arranged multi BGO-SiPM-panel with gamma-ray detectors that are having directional sensitivity to be used in the radiological searches for the low-altitude applications was mounted on an un-manned aerial (UASs) system and the systems signal outputs are processed by a FPGA for the estimation methods Maximum Likelihood Estimation, Matched Filtering and Weighted Symmetry for finding the direction. The minimum activity that the system can detect for a ^{137}Cs source at 1 m distance for 60 s period was measured as 1.3 μCi and direction estimation performance was calculated with 2.3° accuracy [20]. The Bayesian based algorithm was also used for localizing the orphan sources by using mobile gamma spectrometry. The HPGe detector mounted vehicle system was tested with the ^{131}I , ^{133}Ba and ^{137}Cs gamma radiation sources. The method performed estimation success for activity within 50% and location within 27% uncertainty [21]. A detector with a 0.1 L cylindrical NaI(Tl) scintillator was mounted on (UASs) for gamma radiation mapping and source localization. The minimum source detectable height for UAV is almost 10 m for the ^{137}Cs test sources with 35 MBq and 350 MBq activities. The results show that UASs have advantage for hard terrain condition mapping against terrestrial robots. [22]. An alternative direction sensitive system was the rotating scatter mask (RSM) concept that uses a low-Z polyethylene mask located over a position-insensitive detector and energy spectra was recorded with accordance to the geometrically varying blocking mask while the mask rotated at a constant speed. The position dependent spectra were recorded and the detector response curves (DRCs) were constructed to be used for identifying the source direction [23]. For reducing linear dependence of DRCs' using optimization of the mask's shape geometry, three following methods were suggested: The eigenvector approach, the binary method and the modified Hadamard approach were used for the rotating encoding mask types. The Eigen and Spartan general design classes were developed to create the RSM geometries [24]. In the previous studies the Mace mask that reduces the

similarities between the modes was developed. A new design class was simulated and compared to the Mace mask design by evaluating the differentiability of directed modes using the modal assurance criterion. It has the disadvantage of a reduced field-of-view but also can decouple the source directions angular components and improves the average criterion value [25]. Another study utilized an algorithm to evaluate the List Mode Maximum Likelihood Expectation Maximization (LM-ML-EM) imaging techniques using a position-sensitive portable radiation device (COCAE). The source-to-detector distance was then determined using three distinct algorithms: a) the photo-peak count information from each detecting layer, b) the quality of the reconstructed source image, and c) the triangulation method, which was based on the photo-peak count information from each detecting layer for point-like radioactive sources located at various orientations and distances and simulation. In this study, we present a homemade portable gamma radiation detector unit that is capable of working both as a gamma counter and finding the position angle of the existing radiation source. The system consist of a designed detector probe head, electronic blocks (LNA(low noise amplifier), filters, inverter and high voltage power blocks, and FPGA boards), HMI touch screen and user interface for displaying measurements and radiation source position numerically and also by a 360 degree scale, FPGA unit and VHDL based embedded software capable of parallel processing and an algorithm for interpreting the concurrent measurements and estimating the angular position of the gamma radiation source in degree base with respect to the detectors position. It also gives quick response after powering on and provides almost $\pm 45^\circ$ success in angular position of the radiation source. The proposed detector system functions both as a gamma counter and gamma source direction detector that is capable of measuring in a wide energy range. It is a portable, compact and light weighted device designed for mainly field applications and to be used by surveyors. The system provides remote data access to be used in high activity environment. It has a high accuracy in detection and angular position measurement results. The system also has high performance with a single chip operation that both filters, counts and calculates eight gamma counters concurrently. The device is suitable to be used with robotic systems or unmanned vehicles with its light weight and low power consumption.

2. MATERIAL AND METHOD

The main parts of detector system are detector probe, electronic boards, HMI unit, and metal chassis.

2.1 Detector Probe

The detector probe consists of a lead housing and PIN diode arrays. Among radiation sensors to be used in dosimetry applications, PIN diodes are more preferable with its advantages of high sensitivity, small size, good linearity, high quantum efficiency, quick response time and possibility to use with or without bias voltage depending on photovoltaic mode or photoconductive mode for different applications [27]. High photo and radiant sensitive BPW34 model silicon PIN type photodiodes have been chosen as a detector sensor. Its dimensions are 5.4 mm length, 5.4mm, 4.3 mm width, 3.2 mm height and 7.5 mm² radiant sensitive area. They are low-cost component with respect to the other radiation sensitive semiconductor components [28]. Four BPW34 diodes are connected parallel to increase the detector systems sensitive surface as 7.5 mm² ×4 that provides better detection performance [29]. The light sensitive PIN diodes are optically isolated by heat shrinks for filtering light noise but it causes the disadvantage of preventing alpha ray detection.

Although the active area of the photodiode is constant the width of the depletion layer can be modified by changing the applied reverse bias voltage. The photovoltaic mode provides minimum leakage current but has lower sensitivity due to the lower depletion layer. The photoconductive mode has higher sensitivity due to the increment of depletion layer proportional to the applied bias voltage but this increases the value of leakage current that limits the minimum measurable dose rate level. Also, a wider depletion region reduces the junction capacitance of photodiode. For a basic RC low-pass filter, reducing capacitance increases the cut-off frequency that allows for wider bandwidth that maximize the detectors ability to respond to rapid illumination variations. For these advantages photovoltaic mode was preferred for this design.

However, the increasing temperature also increases the leakage current, the studies show that the PIN diodes are suitable to be used in ambient room temperature. As parallel connection increases the detector area, this also has the drawbacks like increasing the dark current from 2.1 pA to 8.4 pA and also increases the junction capacitance 79.9 pF to sum of four BPW 34 capacitance [30].

The Compton scattering, photoelectric absorption and pair production are main possible interaction mechanisms for radiation detectors that results partially or complete energy transfer of the gamma-ray photon to electron energy. For perceiving the gamma rays in a directional way, surrounding of the photodiode array must be shielded with high Z materials that is preferably lead.

For this purpose, a lead housing detector has been designed and its slots are located in 8 different directions 45° apart from each other where the BPW34 arrays have

been placed. The layout of the PIN diode arrays has been adjusted to detect the gamma ray sources up to three detectors at any angular position as seen in (Fig. 1).

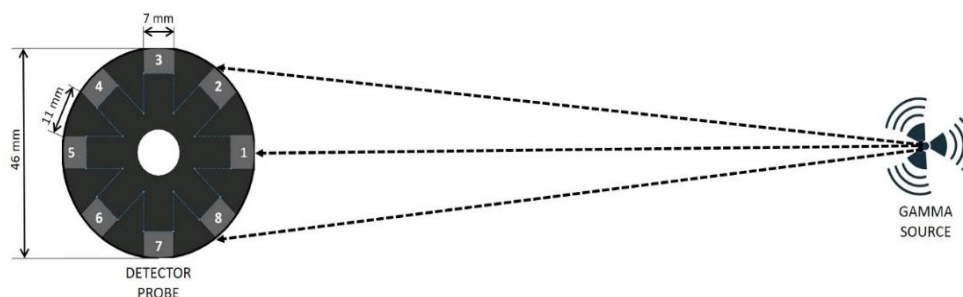


FIGURE 1. Detector PIN diode arrays layout and field of view for a gamma source.

The lead detector housing consists of two parts, the upper cover and the main body. There is a hole in the main body through which the cables from the sensors to the detector are placed. The lead housing has been produced by casting technique by using a 3D printed model as given in (Fig. 2a) for making moulds. The PIN diode arrays are placed in the housing an insulated from the main body and the upper cover of the housing by plastic film and epoxy resin. Each PIN diode array is embedded in the slots located on the lead housing having 11 mm thick separating walls that provides a directional view for the PIN diode arrays. The lead housing has also been covered with a 0.5 mm thick copper plate coated with 0.5 mm tin material to prevent the detection of secondary gamma and X-rays generated by the interactions of incoming gamma rays with the lead material (Fig. 2b). The BPW 34 arrays are placed in the slots of the lead housing as given in (Fig. 2c).

A flexible steel hose is placed between the probe and the unit that is used for holding and adjusting the inclination of the probe and used for shielding the detector cables form electromagnetic noise. For a shielding material with good geometry, the relation of transmitted photons number I and the number without an absorber material I_0 is given as:

$$\frac{I}{I_0} = e^{-\mu t} \quad (1)$$

where μ is the attenuation coefficient and t is the absorber materials thickness. For a bad geometry situation, the equation is modified as:



FIGURE 2. 3D printed mould model (a); shielded and insulated lead housing (b); assembly of BPW 34 arrays (c).

$$\frac{I}{I_0} = B(t, E_\gamma) \cdot e^{-\mu t} \quad (2)$$

where $B(t, E_\gamma)$ is the build-up factor that provides a multiplication correction. The calculated attenuation for the shielding including the build-up factor for ^{137}Cs is almost 70%. The results of the measurements of the angular response of the BPW-34 photodiode detector show that PIN diodes angular response normalized to 0° varies almost less than about 20% for radiation incidence angles $\leq 30^\circ$ [31]. In consideration of these measurements and calculated attenuation, the shielded housing can be evaluated to provide a directional view for the sensors.

2.2 Electronic Boards

The electronic boards consist of the LNA detector boards for 8 channels, power system (high voltage board, battery, digital voltage display and detector voltage adjusting knob), the signal inverter board and the FPGA board units.

2.2.1 LNA Detector Boards

The LNA detector board is an improved version of the circuit used in a thesis [32]. The LNA board has four stages and the rest of the system is given in (Fig. 3).

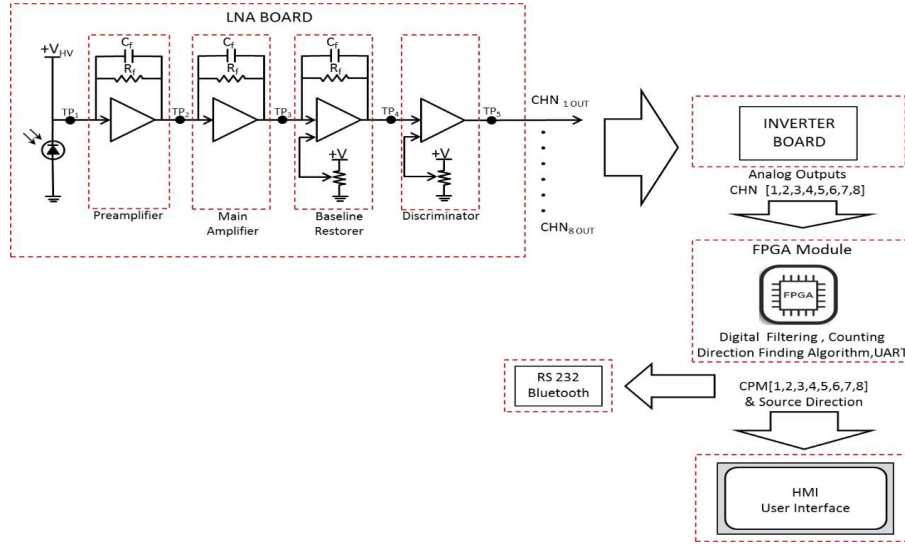


FIGURE 3. Numerical solution of the state-space model.

The preamplifier section of the LNA board operates as a charge to voltage converter and amplifies the charge of sensors into voltage pulses in millivolt levels. In this charge to voltage conversion, it is desired to preserve the waveform of the pulses [33]. In CSA (charge-sensitive amplifiers) the output voltage (V_{out}) is proportional to input charge and its input current (I_{in}) dependency is given by:

$$V_{out} \sim q_{in} = \int I_{in}(t).dt \quad (3)$$

A feedback capacitor C_f and a parallel connected feedback resistor forms a feedback impedance Z_f . The gain (g_{signal}) of the CSA is given by:

$$g_{signal} = \frac{V_{out}}{I_{in}} = -Z_{in} = -X_{C_f} // R_f = -\frac{1}{\frac{1}{R_f} + j\omega C_f} \quad (4)$$

and the decay time constant (τ_{decay}) is given by:

$$\tau_{decay} = R_f C_f \quad (5)$$

So, this gives a short time to obtain a correct charge-proportional voltage. As the detector output rises and falls in a short time, the rise time of the amplifier should be very quick and it should have low inner noise and linear response.

The detector charge output will decrease exponentially in approximately 50 ns. The response of the preamplifier is tested by applying pulses generated by a square wave generator that has rise time less than 10 ns and the rise time of the LNA is measured as 40 ns. Different pulses with increasing voltages applied to test point over the capacitance 1 pF and the amplifiers output have been measured and their logarithmic graph is given in (Fig. 4).

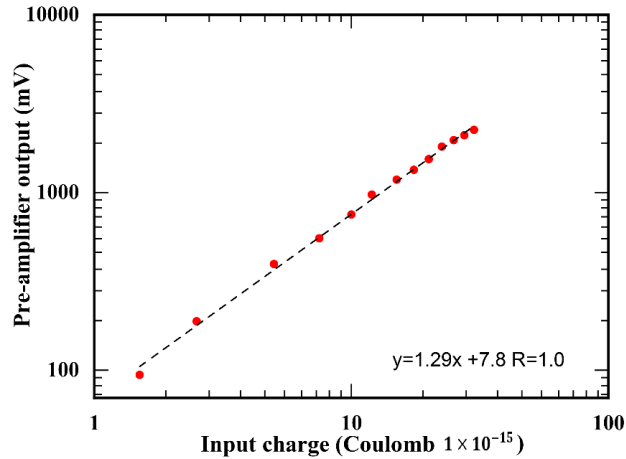


FIGURE 4. Numerical solution of the state-space model.

The second section is the main amplifier part of the LNA board. In addition to amplifying the pulses it also realizes the derivation and integration functions and changes the waveform of the output. By this operations sensor signals are cleared from noise and the fall time is decreased. The logarithmic graph of main amplifiers output voltage v_o versus the charge applied to the input is given in the (Fig. 5).

The third section is the baseline restorer part of the LNA board and used to lower the DC content of the signal to the ground level. This block also transmits and amplifies the signals to the output of the stage that are above the reference voltage which is adjusted by the potentiometer P_1 . The fourth stage is the discriminator section where the discrimination level is adjusted by the potentiometer P_2 and the pulses above this level is transmitted to the output where the lower signals are rejected. The signals are measured by a HAMEG 2524 model 250 MHz digital oscilloscope and a screenshot of the LNA's preamplifier, main amplifier, baseline restorer, discriminator stages output waveforms are given in (Fig. 6), respectively.

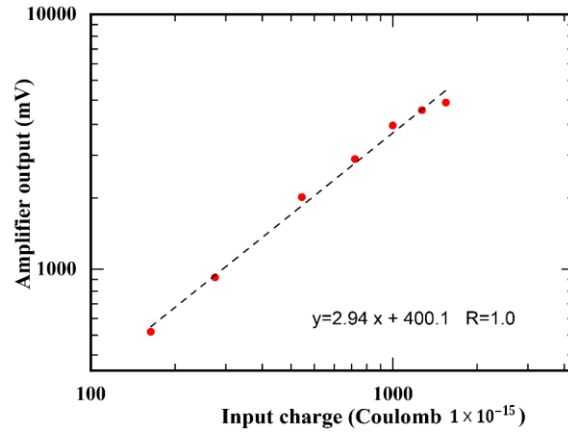


FIGURE 5. Amplifier stage charge to voltage conversion.

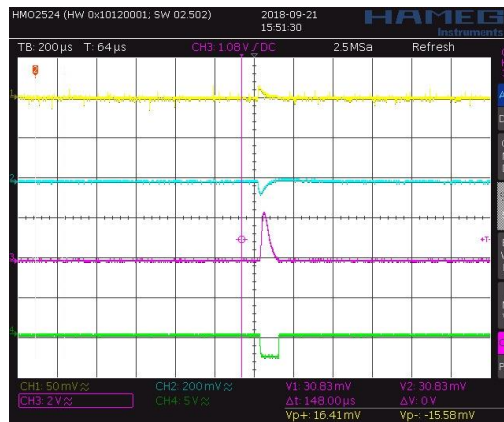


FIGURE 6. Output waveforms of the LNA’s preamplifier, main amplifier, baseline restorer, discriminator Stages for a gamma interaction

The LNA is tested by increasing the frequency of square wave signals and results show that it can count up to 78 K pulses. When the PIN diode is exposed to a gamma source, the pulse width of the discriminator is measured from the scope and its value is found almost 30 microseconds. If this value is assumed to be the dead time of the counter, it can be assumed that the counter can count up to 35.000 counts/sec for this sensor type. The P1 is set to the position for the best measurement and the noise level of the discriminator input from the scope is measured almost ± 46 mV. The P2

potentiometer value is also set accordingly to prevent the triggering of the discriminator by false measurements. Every LNA board is calibrated by using ^{137}Cs gamma source. Their baseline restorer and discriminator levels are calibrated by P_1 and P_2 potentiometers respectively. The power consumption of each LNA board is measured as 12.8 mA.

2.2.2. Detector Power System

12 V DC battery that provides portability and noise free operation. The maximum current value for the system has been measured as 247 mA with 12 V battery. The battery is also used for powering system and a DC-DC step-up high voltage board is used to invert 12V to up to 80 V to be applied detector feeding terminals of the LNA board. Feeding voltages at different voltage levels have been applied and an optimum level of 80 Volts has been chosen. 60V of the feeding voltage has been spent on the resistance and only 20 Volt of the input voltage has been applied over the PIN diode. The detector voltage is adjusted by the voltage knob and its voltage level is measured and displayed on the seven-segment display located in the front side of the detector. This provides an option to use various PIN diode detectors with different bias voltage levels and observe its effect on the detector efficiency and measurement noise.

However, the detector efficiency increases proportionally to the voltage increment, it also increases the noise and causes false detections. The measured noise level in the input of discriminator port in a radiation free environment have almost been almost ± 38 mV. The calibrations are done by setting the optimum operating points where the measurements are maximum and there is no pulse signal output when the gamma source is removed. Discriminator voltage is set to 46mV for filtering noise. Output signals of a single detector and LNA for a ^{137}Cs test source is given in (Fig. 7).

2.2.3 Signal Inverter Board

For this detector design, FPGA with IO's operating only in positive 0V-3.3 V voltage range has been chosen. The analog output pulse of LNA is negative and they have to be inverted into positive pulses and limited in the FPGA input range for counting. An inverter board with 8 channels is also designed to invert the negative pulses to positive scaling to the FPGAs 3.3 V level.

2.2.4 FPGA Unit

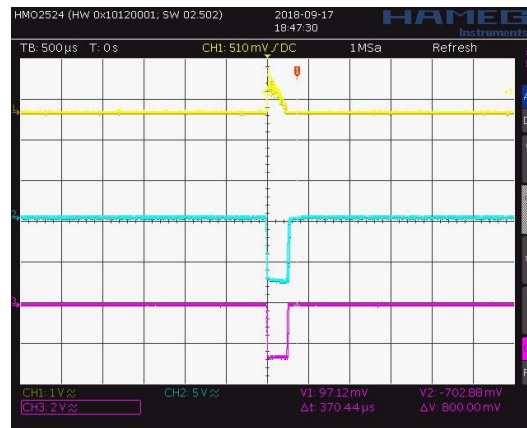


FIGURE 7. Numerical solution of the state-space model.

The system is based on the concurrent measurement of 8 gamma count based radiation detectors. In high activity environment, the detector output pulses increase and also the due to the narrow pulse width, the counter part of the detectors must be capable of operating with high frequency and high precision. The system requires 8 processors for each channel and a master processor for evaluating the measurements and calculating the angle. For meeting these requirements of the system, a XILINX Spartan 3E FPGA chip that is capable of parallel processing has been used. An individual module for each channel and other functions has been created by the gates and FPGA provides a single chip operation. The system code is written in VHDL language. The system has 8 independent, parallelly operating, concurrently running counter blocks embedded in the FPGA and results are calculated and refreshed in every minute. The FPGA has a 50 MHz clock frequency and the sampling period is set to $2\mu\text{s}$. A signal conditioner block has written in VHDL to be used in every channel including filtering, metastability, debouncing, oversampling preventing and rising edge detection blocks for detecting signals with valid durations. However, the system can measure and display counts per second (cps). The measurements are usually fluctuating due to non-uniform exposure of radiation source. For providing a stable and more reliable angular values, counts are converted in counts per minute (cpm). The first cpm value can be displayed after a period of one minute. In order to give an early value before one minute is up, the measurements of each second beginning from the first second to the fifty-ninth second are multiplied by an appropriate coefficient and normalized to the one-minute value. By this option, the system starts displaying cpm since the power is on. The cpm value is calculated by the moving window technique and storing cps values FIFO data buffer. The counted cps values are updated every second.

In every second, the cpm values of 8 channels is updated and displayed and channels are given as CH_k and counts are given as cpm_k , where k is the channel indice and $k=[1,2,3,\dots,8]$, respectively. The first array is placed in 45° and the rest are placed 45° apart from each other. The direction of each array can be calculated by multiplying its array indice value with 45° . In each minute, the cpm values are updated and the cpm results array are evaluated. Among these measurements array, the indice of the maximum value is determined. The Direction of Source (*DOS*) can be calculated by multiplying the indice value “ k ” of the channel where maximum measurement is detected with 45° as given with equation:

$$DOS = k \times 45^\circ \quad (6)$$

For example, if maximum count is received from the channel CH_3 then the result can be calculated by multiplying indice value $k=3$ with 45° , as $DOS= 3 \times 45^\circ = 135^\circ$. However, this approach provides a 45° resolution, the angular resolution can be improved by applying some computational algorithms over the cpm measurements.

2.3 HMI Unit

A 5" NEXTION HMI is used for displaying the cpm and the detected source direction values that are serially transmitted to HMI from FPGA unit. Its user interface is designed and coded to display the counts received from the sensors, maximum count value, calculated angle of radiation incidence of source rays in accordance with the sensors zero angle point, a 360° scale that displays the direction of the source and buttons to navigate between the pages that display results in either cpm or cps units.

2.4 Metal Chassis

As the measurement is so sensitive and the detector signals levels are very low, the system is placed in an aluminum bag with dimensions $32 \times 23 \times 15.5$ cm dimensions. The metal chassis is chosen for shielding electromagnetic noise and grounding. Metal mounting plates are also designed and manufactured for assembling the electronic hardware in the bag and isolating the electromagnetic noise interference between power, processor and LNA sections of the device. The whole detector assembly and its inside view is given in (Fig. 8a) and (Fig. 8b), respectively. The removable metal separator cover placed on the analog part helps to prevent the electromagnetic interference between the analog and digital blocks. In addition, calibration can be performed by reaching the trim pots of the baseline restorer and comparator parts of the LNA cards through the slit window on this cover part.

Additional mounting plates are placed inside the metal case to install the electronics. LNA cards are placed on the upper part of this system so that they can be easily removed and installed by their mounting parts. In the lower part, battery and high voltage cards are mounted. The total weight of the portable unit is measured as 3185 grams. The electronic system and metal assembly is given in (Fig. 9).



FIGURE 8. Detector unit assembly (a); Interior view of the detector (b).



FIGURE 9. The electronic system and metal assembly.

3. RESULTS AND DISCUSSION

3.1 The Calibration

The calculations are based on comparison of cpm values from sensors having efficiencies identical to each other. For providing this condition firstly the backgrounds of the sensors are measured in a radiation source free environment and then the sensors are exposed to the same ^{137}Cs source from 2 cm distance and their cpm measurements are recorded for 15 minutes. The average counts of the sensors are calculated taking into account the background noise and each channels background count are subtracted from cpm values. The counts of every channel are recorded and their average cpm values (cpm_{avg}) are calculated. The ratios of each sensor over this average value are calculated and an array of calibration coefficients ($coef$) are calculated as given below:

$$cpm_{avg} = \sum_1^k cmp_k \quad , k = [1, 2, 3, \dots, 8] \quad (7)$$

$$coef_k = \frac{cmp_k}{cpm_{avg}} \quad (8)$$

The coefficients are multiplied by the actual cpm measurements (cpm_{act}) and corrected cpm values (cpm_{cor}) are evaluated for each sensor. The direction calculation algorithm is applied over these corrected count values and the source position direction is determined by the detector system.

3.2 Detector Tests

The efficiency of the detector was tested with the gamma sources. The experiments were performed in Institute of Nuclear Sciences, Ankara University. For measurements, a hand-made measuring mechanism consisting of a source holder apparatus that radiation source was attached and a rail with a length scale on it, which allowed the source to be positioned at the desired distance by sliding freely on it, was used as given in (Fig. 10).

Two types of test were performed; cpm vs distance measurements for different radioactive sources and source position angular measurements.



FIGURE 10. Source holder and sliding rail.

3.2.1 Cpm vs Distance Measurements For Various Radioactive Sources

The measurement sensitivity of the detector for radioactive sources (^{241}Am , ^{137}Cs , ^{60}Co) with various energy is tested by applying exposure to the detector. The used sources are given in (Fig. 11).

FIGURE 11. Radioactive sources (^{241}Am , ^{137}Cs , ^{60}Co).

Low activity laboratory point sources were used for radiation safety. The activity values and gamma ray energies of the used gamma ray test sources are listed in the Table 1.

TABLE 1. The activity and gamma ray energy of the gamma ray test sources.

Source Type	^{241}Am	^{137}Cs	^{60}Co
Activity	9.761 μCi	3.7 MBq	1 μCi
Energy	59.54 (keV)	661 (keV)	1173 (keV) and 1332 (keV)

^{60}Co source having highest gamma ray energy and ^{241}Am source having lowest gamma ray energy were chosen for determining the detectors energy measurement range.

Each test sources were positioned in front of the detector and counted one by one. Each measurement was taken for 5 minutes and their average cpm measurements was recorded. cpm measurements versus distance was taken by moving the gamma radiation sources position in 1 cm steps. The measurement range mainly depended on the activity of the gamma ray source. It was observed that the cpm values taken according to increasing distance measurements decreased inversely proportional to the square of the source distance in accordance to inverse square law [34] as given:

$$\Phi \propto \frac{1}{r^2} \quad (9)$$

where Φ is the radiation flux and r is the distance value between the radiation test source and the point where radiation flux is to be calculated.

The cpm values versus distance of the ^{241}Am , ^{137}Cs , ^{60}Co sources are given in (Fig. 12), (Fig. 13) and (Fig. 14), respectively.

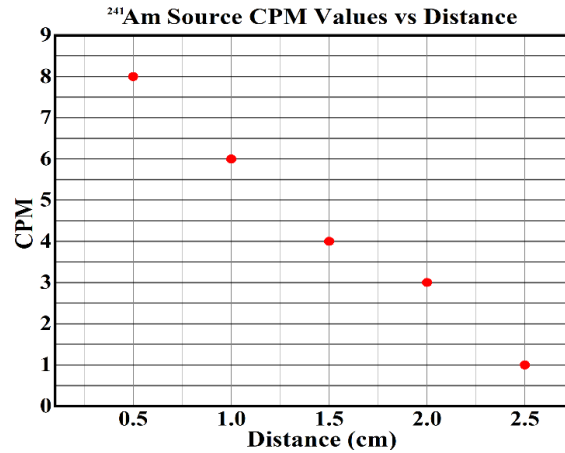


FIGURE 12. ^{241}Am source cpm values vs distance.

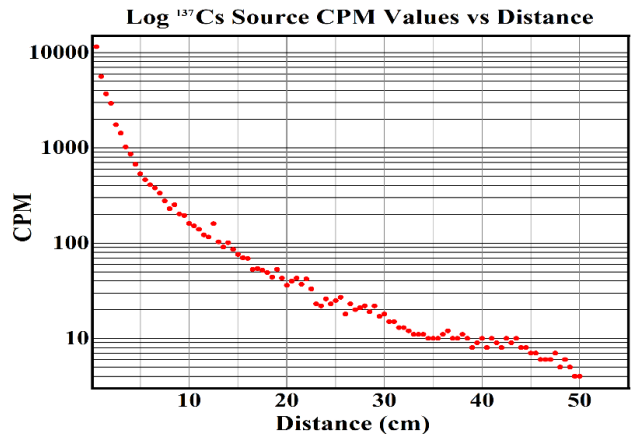


FIGURE 13. Logarithmic ¹³⁷Cs source cpm values vs distance.

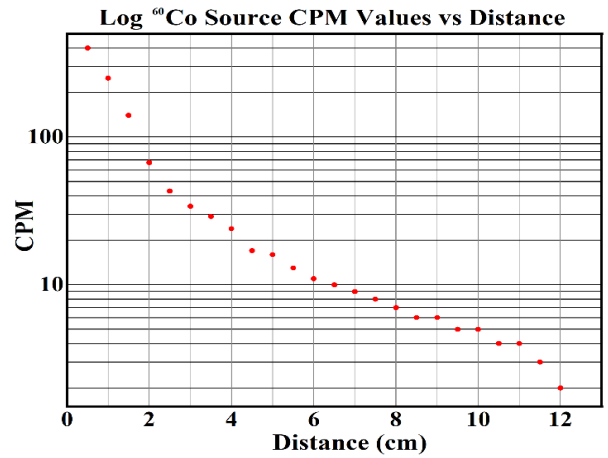


FIGURE 14. Logarithmic ⁶⁰Co source cpm values vs distance.

The test results show that the system can detect gamma rays within the range starting from 59.54 keV to 1332 keV and it operates as a gamma detector and gamma counter unit. The cpm values decrease inversely proportional to the square of the gamma ray test source position distance due to the inverse square law and the detector distance range can be increased by using sources with higher activity.

3.2.2 Source Position Angle Measurements

In the next step, the detector probe was placed in the center of a 360° protractor scale for performing the angular measurements of the equipment. The measurements were taken by increasing angle from 0° to 360° with 10° steps. For every angle steps the cpm and radiation source angle values were measured by moving the radiation source located in the holder mechanism away from the center of the probe in 1 cm steps for the distance values 0 cm to 50 cm. For every angle position the sliding radiation source holder aligned and positioned to the measurement angle with respect to the angle scale on the protractor. The system measures all eight channels concurrently and detects the channel with the highest cpm values. After this the incidence angle were calculated by using the indice of the channel with maximum count and the result were numerically displayed and also shown on the digital scale of the user interface. The measurement results were plotted in a 360° scale vs distance as shown in (Fig. 15). As can be seen from the results in the graph (Fig. 15), it can be said that the detector has successfully detected the angle where the ¹³⁷Cs radiation source is placed for the test. Although the angle detection performance of the system was within acceptable limits, some deviations were detected in some measurements. In order to examine the performance of the tested system in detail, the angular measurements were drawn versus distance for ±10° measurement intervals in 360° scale. The most of the results are within ±45° interval. 14 of 1800 angle measurement is out of this interval and its success is 99.22 %.

- i. The false measurements are shown with red legends. These measurements are concentrated at positions closer to the center. The source has a high activity and the gamma flux is increasing when the source is closer to the sensors. The gamma source is located on the tip of an aluminum cylinder located in the center of the disc and it was hard to handle and manage its orientation to the required angle. The source was aligned in each step but even the smallest angular deviations made during the placement of the point source cause a larger angular difference in calculations due to higher flux at close positions. This may be the reason for the false measurements.
- ii. According to the graph it is seen that some of the angular measurement values of 20°, 110°, 160°, 250°, 290°, 340° were deviated from source angular positions. However, the detectors have directional view, incorrect measurements may occur due to the high cpm values at close range at angles 67.5°, 112.5°, 157.5°, 202.5°, 247.5°, 292.5° and 337.5°, which are the intersection values of the viewing angles of neighboring detectors. This may be the reason for false measurements that are taken for the angular positions close to these intersection angles and source positions close to the detector center.

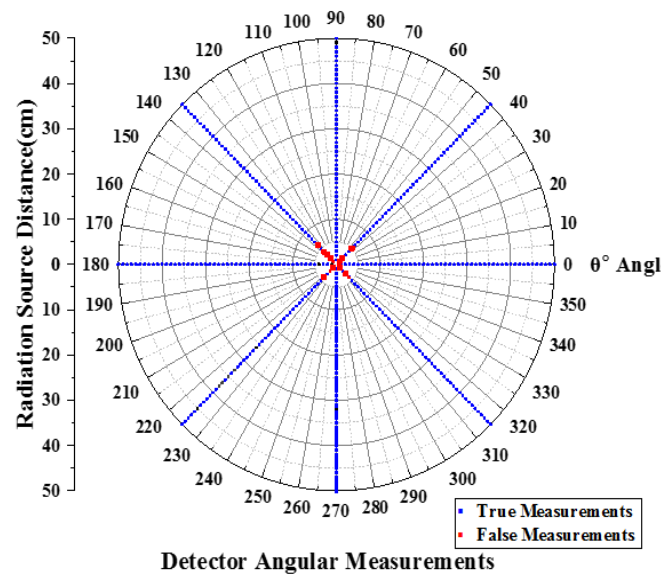


FIGURE 15. Distance vs angular measurements.

- iii. The solid angle seen by the sensor decreases and becomes sharper as the source gets further away. As a result of this, it is observed that the detector's angle estimation performance increases as the source moves further.
- iv. After detecting the direction within 45° , a more precise angle value be determined by rotating the detector till it is aligned with the source position angle and reaches the maximum cpm count. Angular detection performance can be improved by applying this technique.

4. CONCLUSIONS

In this study, an ionizing radiation detector system that can both detect the ionizing gamma source and estimate direction of the radiation source numerically and also can display the direction angle on a scale has been designed, its prototype was manufactured and tested with radioactive sources. It has been observed that the device is capable of measuring in a wide range of gamma sources like ^{241}Am that has the lowest energy, to ^{60}Co that has highest energy. The system also operates as a gamma counter device and takes cpm measurements concurrently with 8 individual channels. The device has also been tested with a ^{137}Cs source for positions at angles ranging from 0° to 360° and for different distances ranging from 0 cm to 50 cm and

36×50 measurements were taken. The results have showed that the device can accurately determine the direction where the radiation source is located. Although the device has initially been manufactured a little bigger for a prototype design purpose, it is still a light, portable and compact hand-held detector unit. It is possible to manufacture the detector with less than half of the existing dimensions by using surface mounted circuit elements and multi-level cards if desired. With its low power consumption, portable design and light weight, this system can be used in the field as a handheld detector by surveyors, can be mounted on air and over land vehicles. It is also suitable to be mounted on radiation survey robots and provide angular data to reach the source directly. The system can be used at security crossing points for safety purposes. By the serial data port and Bluetooth on it, the system enables remote data reading in high-activity risk areas where researchers cannot approach or cannot stay for a long time due to high radiation exposure.

The suggested detector unit is a multisensor system that can count incident rays over each sensor concurrently. The angular resolution can be improved by applying computational algorithms over the evaluated cpm results. Both of the range and efficiency of the detector system can also be improved by using scintillator crystal coupled PIN diodes with larger detection surface. The weight and the dimensions of the system can be reduced by using SMD components multilayer boards to be used in UAVs, robotic system or to be used in field by surveyors. However, this system is based on a Geiger-Müller gamma counting method, the system can also be used as an isotope identifier after adding a proper analog to digital converter (ADC) to the output of the low noise amplifier block.

Author Contribution Statements Conceptualization, Methodology, Software, Electronic-Mechanic Design and Manufacture, Data Curation, System Manufacture, Performing Experiments, B.Ç.; Writing-original draft, Writing-review & editing, Evaluation of the Results, Validation, B.Ç. and H.G.İ.; All authors have read and agreed to the published version of the manuscript.

Declaration of Competing Interests The authors declare that they have no known competing financial interests or personal relationships that could have appeared to influence the work reported in this paper.

Acknowledgments We thank to Ankara University Institute of Nuclear Sciences for their support in providing radiation sources and laboratory in our experiments. This research did not receive any specific grant from funding agencies in the public, commercial, or not-for-profit sectors.

REFERENCES

- [1] IAEA-TECDOC-804 Methods to identify and locate spent radiation sources. (2021, May 24). https://www-pub.iaea.org/MTCD/Publications/PDF/te_804_prn.pdf
- [2] Kroeger, R.A. et al., Spatial resolution and imaging of gamma rays with germanium strip detectors, *SPIE*, 2518 (1995), 236. <https://doi.org/10.1117/12.218379>
- [3] Kroeger, R.A., Gehrels, N., Johnson, W.N., Kurfess, J.D., Philips, B.P., Tueller, J., Charge spreading and position sensitivity in a segmented planar germanium detector, *Nucl. Instrum. Methods Phys. Res. A*, 422 (1999), 206-210. [https://doi.org/10.1016/S0168-9002\(98\)01095-X](https://doi.org/10.1016/S0168-9002(98)01095-X)
- [4] Kroeger, R.A., Johnson, W.N., Kurfess, J.D., Philips, B.F., Gamma ray polarimetry using a position sensitive germanium detector, *Nucl. Instrum. Methods Phys. Res. A*, 436 (1999), 165-169. [https://doi.org/10.1016/S0168-9002\(99\)00615-4](https://doi.org/10.1016/S0168-9002(99)00615-4)
- [5] Kurfess, J.D., Johnson, W.N., Kroeger, R.A., Philips, B.F., Wulf, E.A., Development and applications of position-sensitive solid-state gamma ray detectors, *Nucl. Instrum. Methods Phys. Res. A*, 505 (2003), 256–264. [https://doi.org/10.1016/S0168-9002\(03\)01064-7](https://doi.org/10.1016/S0168-9002(03)01064-7)
- [6] Vetter, K., Burks, M., Mihalescu, L., Gamma-ray imaging with position-sensitive HPGe detectors, *Nucl. Instrum. Methods Phys. Res. A*, 525 (2004), 322–327. <https://doi.org/10.1016/j.nima.2004.03.087>
- [7] Gerl, J., Korten, W., AGATA technical proposal, GSI Report, Darmstadt, 2001.
- [8] Deleplanque, M.A., et al., GRETA: utilizing new concepts in γ -ray detection, *Nucl. Instrum. Methods Phys. Res. A*, 430 (1999), 292-310. [https://doi.org/10.1016/S0168-9002\(99\)00187-4](https://doi.org/10.1016/S0168-9002(99)00187-4)
- [9] Milechina, L., Cederwall, B., Performance considerations for g-ray tracking detectors, *Nucl. Instrum. Methods Phys. Res. A*, 525 (2004), 208-212. <https://doi.org/10.1016/j.nima.2004.03.047>
- [10] Fujimoto, K., Noda, Y., Gamma ray direction finder, *Radioact. Environ.*, 7 (2005) 118-125. [https://doi.org/10.1016/S1569-4860\(04\)07012-3](https://doi.org/10.1016/S1569-4860(04)07012-3)
- [11] Fujimoto, K., A simple gamma ray direction finder, *Health Phys.*, 91 (2006), 29-35. <https://doi.org/10.1097/01.HP.0000196113.49929.be>
- [12] Tajima, H., et al., Design and performance of the soft gamma-ray detector for the NeXT mission, *IEEE Trans. Nuc. Sci.*, 52 (6) (2005), 2749-2757. <https://doi.org/10.1109/TNS.2005.862776>
- [13] Shirakawa, Y., Development of a direction-finding gamma-ray detector, *Nucl. Instrum. Methods Phys. Res. B*, 263 (2007), 58-62. <https://doi.org/10.1016/j.nimb.2007.04.056>
- [14] Shirakawa, Y., Yamano, T., Kobayashi, Y., Remote sensing of nuclear accidents using a direction finding detector, 35th Annual Conference of IEEE Industrial Electronics, 2009. <https://doi.org/10.1109/IECON.2009.5414850>
- [15] Dung, T.Q., Thanh, N.D., Tuyen, L.A., Son, L.T., Phuc, P.T., Evaluation of a gamma technique for the assay of radioactive waste drums using two measurements from opposing directions, *App. Radiat. Isot.*, 67 (2009), 164-169. <https://doi.org/10.1016/j.apradiso.2008.08.008>

- [16] Hindi, M.M., Klynn, L., Demroff, H., Gamma vector camera: A gamma ray and neutron directional detector, IEEE Conference on Technologies for Homeland Security, 2008. <https://doi.org/10.1109/THS.2008.4534502>
- [17] Schemm, N., Balkir, S., Hoffman, M.W., Bauer, M., A directional gamma ray detector using a single chip computational sensor, IEEE Sensors, 2011. <https://doi.org/10.1109/ICSENS.2011.6127024>
- [18] Wahl, C.G., He, Z., Gamma-ray point-source detection in unknown background using 3D-position-sensitive semiconductor detectors, *IEEE Trans. Nuc. Sci.*, 58 (3) (2011), 605-613. <https://doi.org/10.1109/TNS.2011.2113355>
- [19] Akkoyun, S., A method for determination of gamma-ray direction in space, *Acta Astronautica*, 87 (2013) 147-152. <https://doi.org/10.1016/j.actaastro.2013.02.012>
- [20] Becker, E.M., Farsoni, A.T., A multi-panel direction-sensitive gamma-ray detector for low-altitude radiological searches, *Nucl. Instrum. Methods Phys. Res. A*, 836 (2016), 13-21. <https://doi.org/10.1016/j.nima.2016.08.011>
- [21] Bukartas, A., Finck, R., Wallin, J., Rääf, C.L., A Bayesian method to localize lost gamma sources, *App. Radiat. Isot.*, 145 (2019), 142-147. <https://doi.org/10.1016/j.apradiso.2018.11.008>
- [22] Gabrlik, P., Lazna, T., Simulation of gamma radiation mapping using an unmanned aerial system, *IFAC Papers OnLine*, 51 (6) (2018), 256-262. <https://doi.org/10.1016/j.ifacol.2018.07.163>
- [23] FitzGerald, J.G.M., A rotating scatter mask for inexpensive gamma-ray imaging in orphan source search: Simulation results, *IEEE Trans. Nuc. Sci.*, 62 (1) (2015), 340-348. <https://doi.org/10.1109/TNS.2014.2379332>
- [24] Holland, D.E., Bevins, J.E., Burggraf, L.W., O'Day, B.E., Rotating scatter mask optimization for gamma source direction identification, *Nucl. Instrum. Methods Phys. Res. A*, 901 (2018), 104-111. <https://doi.org/10.1016/j.nima.2018.05.037>
- [25] Olesen, R.J., O'Day, B.E., Holland, D.E., Burggraf, L.W., Bevins, J.E., Characterization of novel rotating scatter mask designs for gamma direction identification, *Nucl. Instrum. Methods Phys. Res. A*, 954 (2020), 161232. <https://doi.org/10.1016/j.nima.2018.09.067>
- [26] Karafasoulis, K., Zachariadou, K., Seferlis, S., Kaissas, I., Lambropoulos, C., Loukas, D., Potiriadis, C., Simulated performance of algorithms for the localization of radioactive sources from a position sensitive radiation detecting system (COCAE), 11th International Conference on Applications of Nuclear Techniques, (2011). <https://doi.org/10.1063/1.3665338>
- [27] Bueno, C.C., Gonçalves, J.A.C., de Magalhães, R.R., Santos, M.D.S., Response of PIN diodes as room temperature photon detectors, *App. Radiat. Isot.*, 61 (2004), 1343-1347. <https://doi.org/10.1016/j.apradiso.2004.03.064>
- [28] Silicon PIN Photodiode BPW34, BPW34S. (2021, February 23) <https://www.vishay.com/docs/81521/bpw34.pdf>
- [29] Andjelkovi, M.S., et al., Feasibility study of a current mode gamma radiation dosimeter based on a commercial PIN photodiode and a custom-made auto-ranging electrometer, *Nucl. Technol. Radiat. Prot.*, 28 (1) (2013), 73-83. <https://doi.org/10.2298/NTRP1301073A>

- [30] Glenn, F., Knoll-Radiation Detection and Measurement, 4th ed., John Wiley&Sons, USA, 2010.
- [31] Alvarez, J.T., Khoury, H.J., Hazin, C.A., Austerlitz, C., Angular response of a commercial photodiode in secondary standard fields of $^{90}\text{Sr}/^{90}\text{Y}$ beta radiation, *Radiat. Prot. Dosim.*, 66 (1) (1996), 451-453. <https://doi.org/10.1093/oxfordjournals.rpd.a031776>
- [32] Özgen, S., Bir radyasyon sayacı geliştirilmesi ve çeşitli ortamlarda radyasyon ölçümü. M.S. Thesis, Fırat University, (2021). https://tez.yok.gov.tr/UlusalTezMerkezi/tezDetay.jsp?id=89Unyfp_2iJ5Ppy5Yz3Z1A&no=89Unyfp_2iJ5Ppy5Yz3Z1A
- [33] Iniewski, K., Electronics for Radiation Detection, CRC Press, Boca Raton, 2011.
- [34] Ahmed, S.N., Physics and Engineering of Radiation Detection, Academic Press, San Diego, 2007.